LA-UR- 01- -2902

Approved for public release;
distribution is unlimited.

Title: NATURE'S STATISTICAL SYMMETRIES AND ASYMMETRIES,
A CHARACTERIZATION BY WAVELETS AND AN ILLUSTRATION WITH CLOUDS
(Extended Abstract)

Author(s): ANTHONY B. DAVIS,
Los Alamos National Laboratory, Space & Remote Sensing Sciences Group (NIS-2),

Submitted to: Proceedings of 5th International Congress & Exhibition: "Intersections of Art and Science",
Sydney (Australia), July 8-14, 2001,
organized by the International Society for the Interdisciplinary Study of Symmetry (ISIS-Symmetry)

Symmetry: Art and Science
Vol. 7, No. 2, 1996, page_first-page_last

NATURE'S STATISTICAL SYMMETRIES AND ASYMMETRIES, A CHARACTERIZATION BY WAVELETS AND AN ILLUSTRATION WITH CLOUDS

Anthony B. Davis

Name: Anthony B. Davis, PhD, Physics, (b. Montreal, Qué., Canada, 1952).

Address: Space & Remote Sensing Sciences Group (NIS-2), Los Alamos National Laboratory, P.O. Box 1663 (MS C-323), Los Alamos, NM 87545, USA. *E-mail*: adavis@lanl.gov.

Fields of interest: Mathematical geophysics, fractal geometry, multifractal statistics, three-dimensional radiative transfer theory, remote sensing, clouds, extreme atmospheric phenomena, environmental policy and security concerns (music, films, travel, history).

Awards: Performance Award, NASA's Space Flight Center 1997; Performance Award, Los Alamos National Laboratory 1999.

Publications and/or *Exhibitions*: Davis, A. B., Reeves, N. M., and Cahalan, R. F. (1995) Architecture of Clouds - Clouds as Architecture, Scale-Invariance as a Symmetry in Natural Systems and Artificial Environments, In: Darvas, G., and Nagy, D., eds., *Proceedings of 3rd Interdisciplinary Symmetry Congress and Exhibition "Symmetry: Artificial and Natural,"* 08/14-20, 1995, Washington (DC), published in *Symmetry: Culture and Science*, vol. 6 (#1), Int. Soc. for the Interdisciplinary Study of Symmetry (ISIS-SYMMETRY), 137-140.

Abstract: *Wavelets are the mathematical equivalent of a microscope, a means of looking at more or less detail in data. By applying wavelet transforms to remote sensing data (satellite images, atmospheric profiles, etc.), we can discover symmetries in Nature's ways of changing in time and displaying a highly variable environment at any given time. These symmetries are not exact but statistical. The most intriguing one is "scale-invariance" which describes how spatial statistics collected over a wide range of scales (using wavelets) follow simple power laws with respect to the scale parameter. The geometrical counterparts of statistical scale-invariance are the random fractals so often observed in Nature. This wavelet-based exploration of natural symmetry will be illustrated with clouds where asymmetries and broken symmetries are also uncovered. Both symmetry and symmetry-breaking have deep physical meanings.*

1. INTRODUCTION

1.1 The Lasting Symmetries of a Changing World

Planet Earth —our beautiful island in space— is now being observed uninterruptedly by a myriad of instruments which are like as many extensions of our senses. Satellites are our eyes in space, imaging the Earth from afar often in exotic regions of the electromagnetic spectrum. They have been used to capture everything from the intense activity of the cloudy atmosphere to seasonal changes in vegetation, snow-cover, etc. In the midst of this often overwhelming mixture of regular, semi-regular (e.g., El Niño) and outright chaotic and/or turbulent variability, we are now able to detect the small secular trends of global warming and other subtle changes. In many cases, these slow changes are attributable to human activity; in others, where economic ramifications exist, it is a topic of intense debate *[IPCC, 1996]*. Ground-based and airborne instruments are also at work, often monitoring the atmosphere the 3rd (vertical) dimension. "Seeing" through remote sensing is not enough: in-situ instruments are used to probe Gaia the way we smell, taste and actively touch our immediate environment. Data from the depths of the oceans are thus becoming available to subject-matter experts. Turning even more inward, the most minute vibrations of the Earth's crust are being recorded as we "listen" for quakes that tell us volumes about its internal structure. Yet other instruments measure geophysical fields that escape our

perception per se: magnetism, electricity, and gravity studies are nonetheless important in building our understanding of the Earth system, especially in the nearby interplanetary space where the Earth's fields interact with the solar wind.

Although the rationale for all this high-tech scrutiny is scientific rather than artistic, we are discovering that the Earth's complex dynamics obey certain symmetries that are intellectually appealing. However, these are not symmetries in the traditional sense of exact replication of identifiable features under spatial transformations: translations, rotations, mirror-imaging, changes of scale, and all possible combinations thereof. As soon as scale-changes are included, iteration ad infinitum of these operations generically leads to fractal structures *[Barnsley, 1988]*. Biological systems tend to do this in a deterministic or quasi-deterministic fashion, and stunning patterns naturally arise from growth processes: spiral seashells, elegant ferns, Fibonnaci branching sequences, etc. We are more interested here in inanimate matter which is not as "programmed," hence "disciplined." Its symmetries (invariance properties) are therefore purely statistical in kind:

- homogeneity (not to be confused with uniformity, lack of spatial variability) for translations in space that we will denote collectively as D_s (for "Displacements in space");
- isotropy for arbitrary rotations in 2D- or 3D-space and parity (a mirror-symmetry in the parlance of physics) denoted R_2 or R_3 and P respectively; and
- scale-invariance, often associated with "fractality," for zooms (changing the observation scale) denoted Z_s. This is the symmetry we will be most interested in here.

Time of course plays a special role in both living and non-living systems. From cell-biology to philosophy, the one-way sequence of birth → growth → maturation → aging → death is observed or accepted as fundamentally irreversible. In contrast, geophysical systems are often in a state of dynamical equilibrium, hence the notions of

- stationarity (not to be confused with constancy, lack of temporal variability), a property mapped to statistical invariance under translations in time that we will denote D_t (for "Displacements in time");
- invariance under time-reversal (does a time record of observations look statistically similar in the opposite direction?), that we denote T; and
- temporal scale-invariance for "zooms" in time (changing the duration of observation) denoted Z_t. This is another symmetry of significant interest here.

Eastern philosophies, which are even more symmetry-obsessed than their Western counterparts, generally do think of Life (at large) as an intricate cycle of reincarnations. Not surprisingly, there are deep analogies to be explored *[Capra, 1991]* between Eastern mystical traditions and Physics, a product par excellence of the Western world.

1.2 Physics: A Culture of Symmetry

Geophysicists are often, but not always, physicists first. Those that are were inevitably got rigorous training in so-called Hamiltonian systems which obey certain conservation laws, for instance, energy. *Emmy Amelie Noether [1918]* proved a beautiful theorem for such systems showing that for every conserved quantity there is a symmetry (of the fundamental time-evolution equations) under a specific continuous transformation, and vice-versa. Thus energy conservation is mapped to D_t, momentum conservation to D_s, and angular momentum conservation to R_3. In quantum physics, there are other operators and associated symmetries such as "charge conjugation," denoted C, famous for its role in the "CPT theorem" in high-energy physics, that guarantees, by Noether's theorem, conservation of electric charge. Einstein's theories of relativity are now presented most elegantly in terms of geometrical invariants (conserved quantities) such as the space-time interval (or "world-line" element) dx^2-cdt^2. From there, the standard relativistic transformation groups of Lorentz and Poincaré are obtained; these are non-trivial kinematic combinations of D_t and D_s that translate the measurements of one observer to those of another when they are in motion relative to one another. The basic principle of relativity states that the laws of physics must be invariant under these transformations.

This physics of "closed" Hamiltonian systems is routinely used in particle accelerators and for the Universe as a whole. Understandably, it also works for the relatively new cross-discipline of "cosmo-particle" physics. That is, a physics merger of the infinitesimally small and the incommensurably large, although the Universe was actually not very big at the short times after the Big Bang studied by cosmo-particle physicists. However, "merging" does not mean "spans everything in between here. Indeed, when one tries to understand a finite (many-component) portion of the Universe, energy and other quantities are exchanged with the surroundings, and the Hamiltonian paradigm has to be abandoned. In this context, a statistical physics of "open" systems emerges from Hamiltonian physics, simply by accepting that we will never know everything about all the particles and all the fields in the Universe. Symmetry analysis is still a powerful tool, although dissymmetry is often the outcome. For instance, as much as the fundamental Hamiltonian principles are T-invariant, the basic laws of statistical physics are not. To wit, Boltzmann's famous "H-theorem" stating that entropy (a statistical measure of disorder) must increase in time. In the macroscopic world, there is an essential dissymmetry in the "arrow of time." Unless (some higher form of) energy is pumped into a thermal system, heat (thermal energy) will flow from the warm to the cold regions in a natural tendency towards equilibration. This is the "everyday" physics of refrigeration and insulation at work, a constant struggle against the 2nd law of thermodynamics: total entropy must increases. The same tendency works on mass (diffusion and contamination processes), momentum (stress, friction and slippage or catastrophic rupture), charge (electrical resistance or dielectric breakdown and discharge), and so on. This is the world-view of seasoned geophysicists and most engineers. In short, everything is in a constant state of flux.

Symmetry is arguably the most resilient concept in the physicist's mental tool-box. If necessary, it can become an extremely formal abstraction in comparison with the crystallographer's discrete set of translations and rotations (i.e., finite subgroups of R_3 and D_S) or the gemnologist's carefully selected mixtures of transformations in R_3 and P. One can think of Murray Gell-Mann's "Eight-fold Way" that lead to the (now) Standard Model of particle physics *[Capra, op. cit.]*. Even contemplating the non-Hamiltonian world of geophysics, the physicist finds new symmetries to build upon. One of these, scale-invariance, is based on Z_S and Z_t, the collections of all possible zooms in space and time.

Z_S and Z_t are curiously under-explored transformation groups. One interpretation of operations in Z_S and Z_t is in the statement that French and (pre-SI era) British physicists, using patently different systems of physical units, should agree on the formulation of the laws of physics once the experimentation is done. This is less simplistic than first appears. It means that the numbers obtained in measurement do not matter in final analysis, only their ratios are important. So yards are as good as meters ... as long as the two systems are not mixed. In physics, "non-dimensional" numbers reign as absolute monarchs. These are (often quite simple) combinations of quantities that do not depend on what units used to measure each of them, however, they literally dictate the quality of the physics. Take, for instance, the "Reynolds number" in hydro/aero-dynamics $\mathrm{Re} = VL/\nu$ where V is the typical velocity and L the overall size of the flow while ν is an inherent property of the fluid known as "viscosity" (in statistical physics it describes the rate of conversion of stress and strain into thermal energy). If Re is small, the fluid dynamics are "laminar," that is, regularly behaved (smooth) in space and time; if Re is large, then the flow is "turbulent" and then spatio-temporal chaos is the name of Nature's game. Of course, we also understand that the flavor of the prevailing physics changes radically as we freely explore Z_S and Z_t together: going from the ultra-fast sub-atomic world of quantum physics to the mesoscopic world dominated by that "everyday" thermal and thermal-like physics, to the majestically slow and quintessentially relativistic realm of cosmology. So we will often restrict ourselves to a sub-range of scales. This physical limitation of a mathematically unbounded construct is unique to Z_S and Z_t among all possible transformation groups, and we can expect a similar uniqueness in the associated symmetries. In the following, we will use zooms with these understandings in mind: seek relations between non-dimensional numbers within finite ranges of scale.

1.3 Program and Outline

I will present a unified scheme for characterizing qualitatively as well as quantitatively of the most basic symmetries —invariance under D_t or D_S, R_2, and Z_S or Z_t (within limits)— in data from virtually any kind of measurement device. It uses the "wavelet transforms" presented in Section 2 which can be thought of as the mathematical equivalent of a microscope on geophysical "signal." This instrument-of-sorts is used to examine any portion of a sample (a one- or higher-dimensional dataset) at any magnification, within the observational limits. As in the laboratory analogy, it is

handy to have several kinds of microscopes; here, different kinds of wavelets prove useful in different tasks. Section 3 is devoted to scale-invariance, the symmetry of primary interest here. Symmetry violations will also be covered: dissymmetric or asymmetric scale-invariant situations (Section 4) and on broken scaling symmetry (Section 5). Along the way, several practical applications of this kind of data analysis will be described, especially concerning clouds and their optical (solar radiation transport) properties. Wavelets can also be used in stochastic modeling, that is, computer-based generation of synthetic data that has prescribed statistical properties. Again specific applications will be used to illustrate the general idea. Finally, we summarize in Section 6 and look beyond the material presented here.

2. WAVELET TRANSFORMS, ILLUSTRATED WITH CLOUD DATA AND TWO TRANSCENDENTAL NUMBERS

2.1 The Continuous Case: No scale or position is left behind ...

Consider some geophysical variable of interest f, dependent on position in space or time x, that we will denote $f(x)$; in essence, this is a long string of numbers obtained from an instrument or a model calculation. The general philosophy of wavelet analysis is the separation of this signal into a slowly varying, or "local average," part and the remaining fast-varying part, or "fluctuation." In fact, this is often a goal in life generally speaking: how to separate the big-picture from the details, the forest from the trees, etc.

Mathematically, this separation corresponds to two complementary filtering operations. A wavelet filter looks like this

$$T_\psi[f](a,b) = \int \psi_{a,b}(x) f(x) dx, \tag{1}$$

for

$$\psi_{a,b}(x) = \frac{1}{a}\psi\left(\frac{x-b}{a}\right) \tag{2}$$

where a is the scale at which we separate the "fast" and "slow" components and b is a positioning parameter. Note that the $1/a$ factor in Eq. (2) is not the conventional normalization (calling for a $1/a^{1/2}$ factor *[e.g., Mallat, 1999]*) but is convenient in the following statistical considerations. The mathematical shorthand in Eqs. (1-2) is now translated into plain language.

The function $\psi(x)$ is the so-called "mother wavelet" that it is only required to have a vanishing mean value, hence to oscillate at least once around zero; it is usually assumed to take (significantly) non-vanishing values only near or around the origin $x = 0$. Thus, the term $\psi_{a,b}(x)$ in the above equations is a dilated ($a > 1$) or shrunken ($a < 1$) version of the mother wavelet form that is also displaced by a distance b in either direction , to the right ($b > 0$), or to the left ($b < 0$). Notice the built-in connection with Z- and D-transforms respectively. The operation on the r.-h. side of Eq. (1) just means *'form the product of the (scaled/shifted) wavelet and the input signal, then sum over all (available) values of space (or time).'* The result is an "image" of $f(x)$ through the wavelet transformation (WT), based on a certain choice for $\psi(x)$, that will depend on a and b. So the notation $T_\psi[f](a,b)$ on the l.-h. side represents a 2D array of numbers resulting from the operation prescribed on the r.-h. side, with a book-keeping of sorts for all the dependencies it inherits. Another popular notation for the wavelet transform or "coefficient" of $f(x)$ in Eq. (1) is $\langle f,\psi_{a,b}\rangle$.

If the local mean is the desired outcome at scale a, rather than the fluctuation, then one uses a "scaling function" $\varphi(x)$ rather than a wavelet $\psi(x)$. The only difference is that it does not need to oscillate or, more precisely, it should have a non-vanishing mean. Otherwise, the same notations apply: $T_\varphi[f](a,b)$ as in Eqs. (1-2) or $\langle f,\varphi_{a,b}\rangle$.

The l.-h. side of Fig. 1 shows a wavelet and a scaling function for a very simple case: the *Haar [1910]* basis pair. It is composed of one scaling function $\varphi_H(x)$ that takes the average of $f(x)$ over a certain interval and one wavelet $\psi_H(x)$ that takes the difference between the summations of $f(x)$ over the two halves of that interval. The "basis" quality expresses

the fact that these two filters produce independent pieces of information on $f(x)$ at all scales and positions. Notice how $\langle\psi_H,\varphi_H\rangle = \langle\varphi_H,\psi_H\rangle = 0$ which is like stating that the projection of an EW vector onto the NS axis is just a point (has no "weight") and vice-versa. In fact, the word "projection" is often used in a technical sense to describe wavelet filtering operations in high-dimensional function spaces. The r.-h. side of Fig. 1 shows another basis with one scaling function and two wavelets *[Davis et al., 1999]*; the second wavelet (with two oscillations) is known as the "French top-hat."

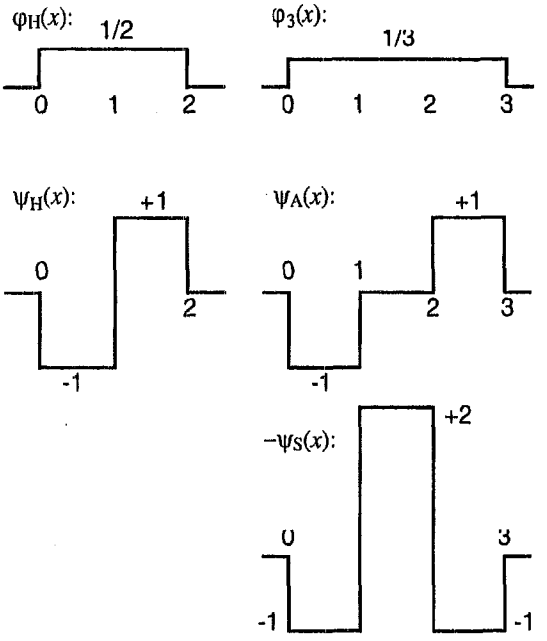

Figure 1: *Wavelet dyad and triad.* On the l.-h. side, the well-known Haar basis pair contains a wavelet and a scaling function; on the r.-h. side, we have a triadic counterpart of the Haar basis with two wavelets, one anti-symmetric and one symmetric, and a scaling function.

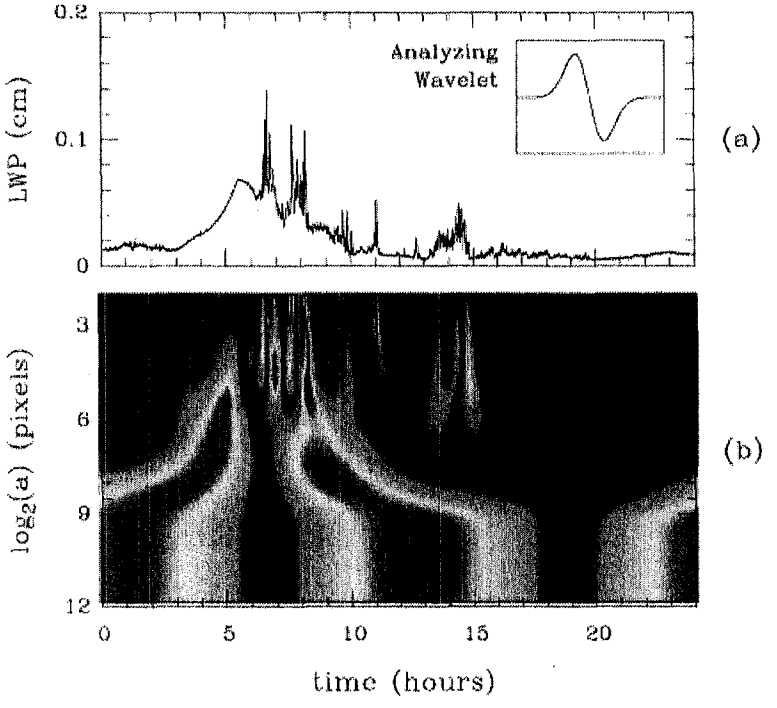

Figure 2: *The continuous wavelet transform.* The top panel shows the 1D input data, a daily record of column-integrated atmospheric liquid water, or liquid water path (LWP) in cm or g/cm^2. The data was obtained from an up-looking 2-channel passive microwave radiometer. The lower panel is the 2D result from Eqs. (1-2) in absolute value displayed on a gray scale.

Figure 2 shows the image of a function $f(x)$ though the continuous wavelet transform (CWT). The graph of $f(x)$ is plotted in the top panel (a); it is a trace in time of the amount of liquid water in the atmospheric column above a instrumental station in Oklahoma for one day. The two-dimensional result from Eqs. (1-2), $T_\psi[f](a,b)$, is illustrated in the lower panel (b) on a gray scale in absolute value, denoted $|T_\psi[f](a,b)|$ in the following section; note that the scale parameter a increases downward. The choice of analyzing wavelet is shown in the inset in panel (a). It is clear that there is much redundancy in the representation of $f(x)$ by its CWT. If we are given all the data in $T_\psi[f](a,b)$ there are many different ways we can reconstruct $f(x)$ *[Daubechies, 1992]*. Reducing this redundancy is one motivation for developing the discrete wavelet transform (DWT), another is the associated computational efficiency.

2.2 The Discrete Case: A Hierarchical Sampling in Scales and Positions

In many applications it is desirable to have a representation of some input function $f(x)$ sampled over N equidistant points on the x-axis that also has N points, rather than the $\approx N^2$ points used to plot Fig. 2b. This is not only possible within wavelet theory but leads to the extremely efficient method of computation called "multi-resolution analysis" (MRA) *[Mallat, 1989]* illustrated in Fig. 3.

Not all possible wavelets are eligible for MRA implementation, but the Haar basis is and it is used in Fig. 3. A binary tree structure in Fig. 3 is used to sample the scales a and the positions b so that $\langle\psi_{a,b},\varphi_{a',b'}\rangle = \langle\varphi_{a,b},\psi_{a',b'}\rangle = 0$ for all the pairs used with $(a,b) \neq (a',b')$. Hence the need for 2^J points; here we use $J = 4$, hence $N = 2^4 = 16$ values of f. First we compute the differences and averages over two samples, move to the next two and repeat these dual operations until we run out of points; at each position, we store the difference (or "detail") and pass the average on to the next scale level. We repeat this at all $J = 4$ levels, producing one overall average and 8+4+2+1 = 15 differences; exactly $N = 16$ numbers are thus stored. These constitute the DWT of the signal, plus its average. The signal in Fig. 3 is made of the 16 first digits in $e = 2.71\cdots$, the base of natural logarithms.

Figure 4 illustrates the inverse DWT where 16 numbers are extracted from storage to reconstruct a signal. The signal restoration procedure starts at the bottom of the binary tree with the overall average and first level difference, then detail is added scale-by-scale, and position-by-position until there is no more detail left in storage. In this example, we have restored the first 16 digits of $\pi = 3.14\cdots$.

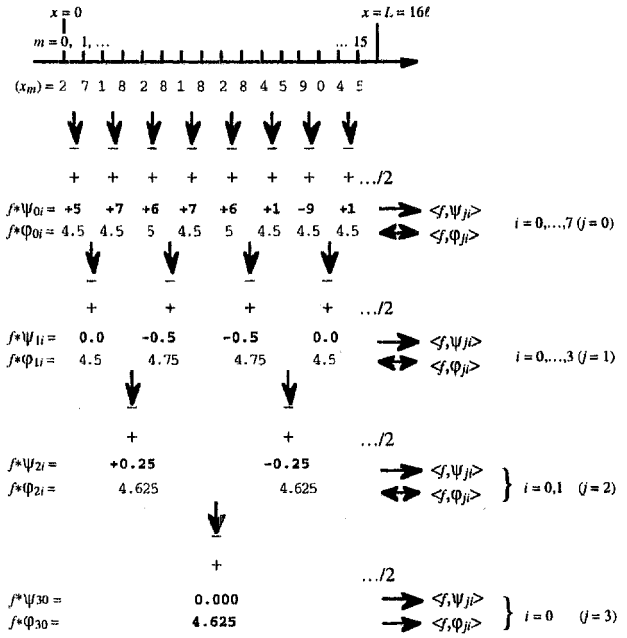

Figure 3: *The discrete Haar wavelet transform.* See text for details.

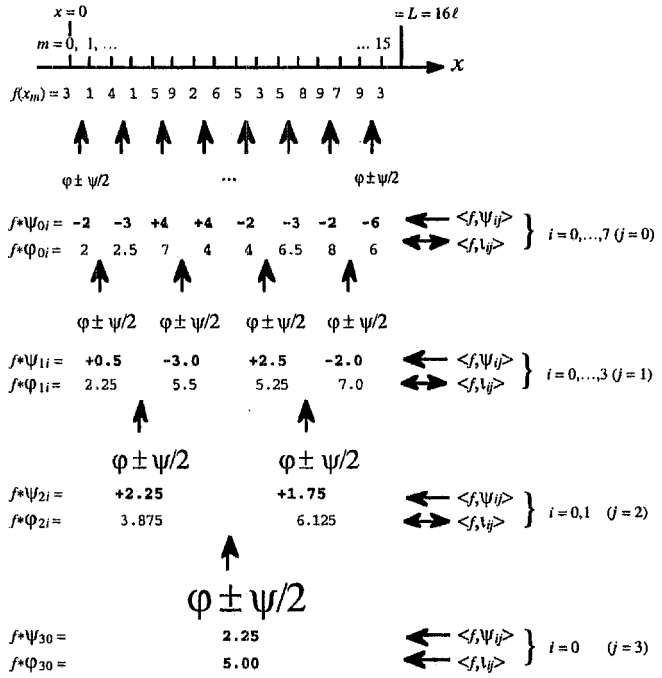

Figure 4: *The inverse discrete Haar wavelet transform.* See text for details.

In both analysis (Fig. 3) and synthesis (Fig. 4) procedures, the number of floating-point operations, better known as "FLOPs," is $2N$. This is less than necessary to compute the mean and standard deviation of a signal. The 3-member basis illustrated on the r.-h. side of Fig. 1 calls for a ternary tree and the corresponding number of FLOPs is also $\approx N$. So a major benefit of replacing the continuous Z- and D-based symmetries of Eqs. (1-2) by discrete ones is the high computational efficiency of MRA.

For a perspective on MRA efficiency, consider that the CWT costs $\approx N_a \times N \ln N$ FLOPs where N_a is the number of scales requested (typically $\approx$N) and $\ln N$ is the natural log of N. For the example in Fig. 2, we have $N = 4320$ (3 LWP samples per minute), hence $\ln N \approx 8.4$ and well over 100 million FLOPs are required for the CWT; this contrasts sharply with the than the 10 thousand, give or take a couple, FLOPs needed for the DWT.

2.3 The Semi-Discrete Case: A few Scales are Enough but all Positions are Potentially Interesting!

In some applications, including spatial the statistics described further on, the sparse sampling of position space associated with the binary tree in Figs. 3-4 is a liability. Indeed, interesting (spatial) events may be missed if one only looks at the wavelet coefficients produced in Fig. 3, even though they suffice to reconstruct the data in Fig. 4. Recall that this is only one of many possible ways of encoding and reconstructing the data.

A compromise here is to use a redundant representation of the data that is not as overwhelming as the CWT in Fig. 2. The idea of using only $J = \lfloor \log_2 N \rfloor$ scales in a-space is retained from the discrete wavelet transform in MRA. We have used $\lfloor X \rfloor$ here to designate the lower-or-equal integer of the number within the brackets, namely, $X = \log_2 N$ which is the unique solution of the equation $2^X = N$. For instance, we have $J = X = 4$ for $N = 16$ and $J = X = 5$ for $N = 32$ while $X = 4.643856\cdots$ for $N = 25$, which leads back to $J = 4$. The number of positions one can sample in b-space depends on the details of the wavelet but it is not much less than N if J is large enough. We thus obtain about $J(N) \times N \approx N \log_2 N$ wavelet coefficients in this semi-discrete WT and, leveraging on the MRA trick, it takes about that many FLOPs to obtain them. For the triadic basis in Fig. 1 (r.-h. side) rather than the Haar basis, we simply replace the 2s by 3s.

Other names for the semi-discrete WT found in the literature *[cf. Fournier, 2000; and references therein]* are "stationary" WT and "translation-invariant" WT but, for reasons that will soon become clear, this nomenclature could be quite misleading in statistical applications. A third alternative, "non-decimated" WT, is acceptable but not as intuitively appealing in symmetry analysis as "semi-discrete."

3. STATISTICAL SYMMETRIES, ILLUSTRATED WITH CLOUDS

3.1 Statistical Scale-Invariance

In observations of geophysical fields or time-series, there are two operationally important length- or time-scales: the total length of the record, L, and the interval between two subsequent samples, ℓ. Thus, the total number of samples in the record is $N = L/\ell$. The scales selected by the dyadic MRA are of the form $a_j = \ell \times 2^j$, for $j = 0, 1, 2, \ldots, J-1$. From there, the positions used in the binary tree for the DWT are $b_{ij} = 2i \times a_j$, for $i = 0, 1, 2, \ldots, 2^{J-(j+1)}-1$. For the semi-discrete WT, the positions are simply $b_{ij} = i \times \ell$, for $i = 0, 1, 2, \ldots, N-(2^j-1)$. This enumeration assumes a Haar or Haar-like dyadic decomposition; similar enumerations exist for the triadic basis in Fig. 1 (r.-h. side).

One of the simplest possible spatial statistics to examine can be denoted

$$S_\psi(q;a) = \left\langle \left| T_\psi[f](a,b) \right|^q \right\rangle_{b,f} \tag{3}$$

where $\langle\cdot\rangle_\chi$ means *'average the quantity inside the triangular brackets (over the variable(s) in the sub-index).'* So $S_\psi(q;a)$ is just the qth-order statistical moment of the absolute ψ-WT coefficients at scale a. In this case, we have averaged over all positions (b-values in WT) and, if possible, over all the different realizations of the random signal f.

If the data is scale-invariant (with respect to zoom operations), then it can be shown *[e.g., Sornette, 2000]* that $S_\psi(q;a)$ must be a simple power-law function of a:

$$S_\psi(q;a) \propto \left(\frac{a}{L}\right)^{\zeta_\psi(q)} \tag{4}$$

where "$\propto$" means *'proportional to'* and the r.-h. side has been non-dimensionalized by using the ratio of a to L. Another scale than L can be used here if more convenient. The important goal here is to capture as much of the dependence of $S_\psi(q;a)$ at once in the same power-law formula: we allow the exponent $\zeta_\psi(q)$ a dependence on q, but the implicit proportionality factor in Eq. (4) should be weakly dependent on q. Examples of $\zeta_\psi(q)$ follow.

The most publicized aspect of scale-invariance is graph self-similarity which follows from Eq. (4) with $q = 1$ *[Mandelbrot, 1982]*. Graph self-similarity is illustrated in Fig. 5 using artificial data known as a "bounded cascade" *[Marshak et al., 1994]* which are best generated using the inverse Haar DWT in Fig. 4. Bounded cascades obey Eq. (4) with $\zeta_\psi(q) = \min\{qH,1\}$ for a broad class of wavelets. Here we have set the parameter H to 1/3. Looking at the r.-h. side of Fig. 5, note how the results of sequential zooms into random portions of data are essentially indistinguishable from one another: this is graph self-similarity. This means that the graph of $f(x)$ is a random fractal object, by extension, $f(x)$ is called a fractal function. The fractal dimension of is graph is given by $D_g = 2-\zeta_\psi(1)$; for the illustrated case, we have $D_g = 5/3$ since $\zeta_\psi(1) = H = 1/3$ whereas any smooth (mathematically speaking, differentiable) function yields $\zeta_\psi(1) = 1$ and has the usual integer dimension $D_g = 1$ of a line. The l.-h. side of Fig. 5 shows the same sequence of zooms but holds the f-axis constant: the variability, i.e., $S_\psi(q;a)$, clearly decreases with scale. This is a sign that $\zeta_\psi(1) > 1$ in Eq. (4), a property known as "stochastic continuity."

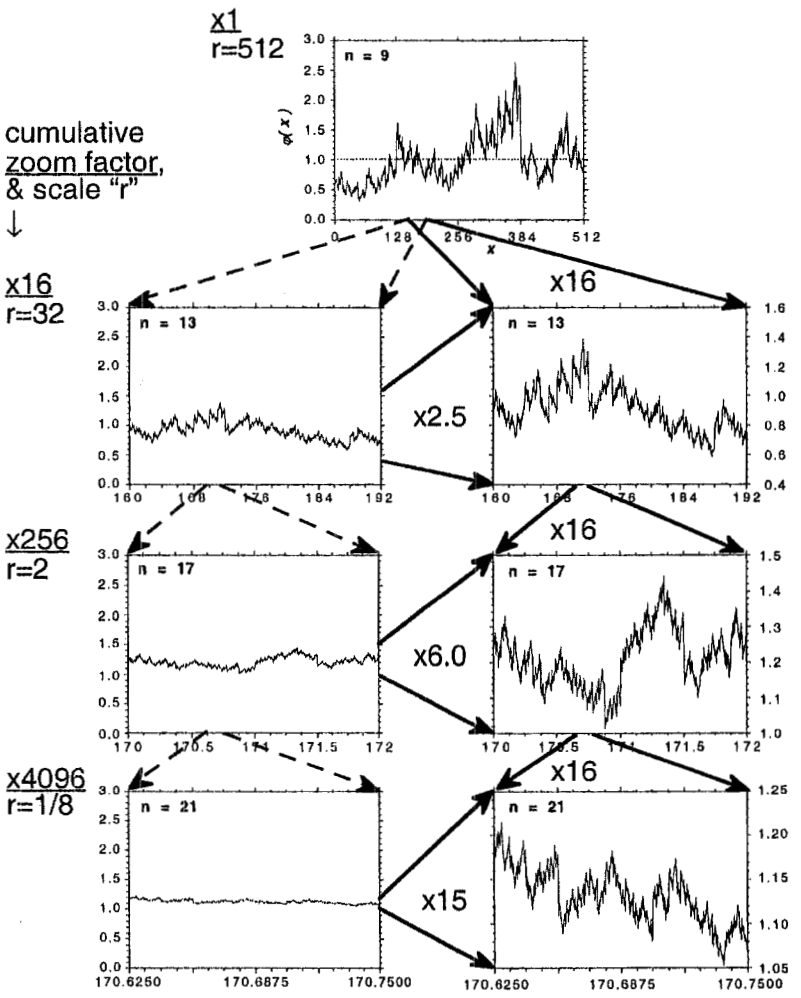

Figure 5: *The self-similarity (r.-h. side) and stochastic continuity (l.-h. side) of a bounded cascade model.* See text for details.

Figure 6a shows typical data on internal cloud structure from long aircraft penetrations into a marine stratocumulus layer. Such persistent and extensive clouds form almost daily off the coast of California and off other Eastern shores of the world's oceans. Because of their ubiquity and strong reflectivity, these cloud systems are important factors in the Earth's climate. From there, we can understand the need to better characterize their internal structure; their outer structure is not very interesting: essentially, a flat top and a flat base. The data is for cloud "liquid water content" (LWC) which measures (in g/m^3) the amount of water contained in the droplets suspended in the cloudy air sampled by a special probe under the wing of an aircraft every 5 meters along the horizontal flight path. Other parameters of interest for marine stratocumulus are: typical cloud thickness of 0.3–0.5 km; altitude is only about 1 km; droplet size is around 10 micrometer (1/100 of a mm) and there are typically 100 droplets-per-cc. If all the water in these clouds was brought to the ground, the depth of the layer would therefore be less than a millimeter thick. Although for a different cloud type, this estimate is consistent with the data in Fig. 2a. The area coverage of marine stratocumulus is generally huge, in the millions of square-km, hence their importance for the regional radiative energy budget. Thus, one such cloud system contains about a billion tons of water in about 10^{23} droplets at any given time!

Figure 6b shows a plot of $\log_{10}S_\psi(2;a)$ versus $\log_{10}a$ for three different choices of the analyzing wavelet ψ, including a "poor-man's wavelet" *[Muzy et al., 1993]* consisting of just the difference between two LWC points separated by a variable distance a: $T_\psi[f](a,b) = f(b+a)-f(b)$ and $S_\psi(2;a) = \langle | f(b+a)-f(b)|^2 \rangle_{b,f}$. This older approach in data analysis restricted to $q = 2$ is known as "structure functions" [*Monin and Yaglom, 1975*] or the "semi-variogram" *[Christakos, 1992; and references therein]*. The tendency of the statistical results to align rather well in the log-log plot shows that scale-invariance prevails, as defined by the power law in Eq. (4). Notice that this is not an exact symmetry by scale-invariance which would mean a perfectly straight line in Fig. 6b. So, in spite of its appearance in Fig. 6a, LWC data has a hidden symmetry, that of scale-invariance. We also note that the exponent $\zeta_\psi(2)$, defined in practice as the slope of the line in Fig.4, is not very sensitive to the choice of wavelet; for more information on why/when this is expected and not, we refer the interested reader to the review article by *Muzy, Bacry, and Arnéodo* [*1994*]. Since we are not in a situation here where the exponent depends critically on wavelet choice, we will sometimes drop the subscript ψ.

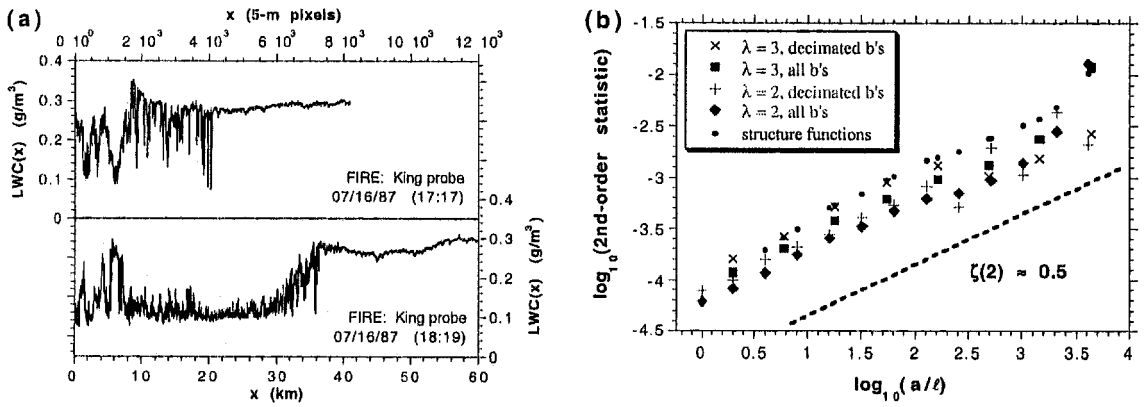

Figure 6: *The scale-invariance of internal cloud structure.* **(a)** Two traces of liquid water content (LWC) or density in g/m^3 obtained from airborne probes during the FIRE'87 field experiment in marine stratocumulus *[Albrecht et al., 1988]*. **(b)** Structure functions and wavelet-based generalizations have similar scaling. Notice the noise in the large scales for ("decimated b's") DWT-based estimates due to poor sampling; the semi-discrete WT used to access all b-values reduces this noise.

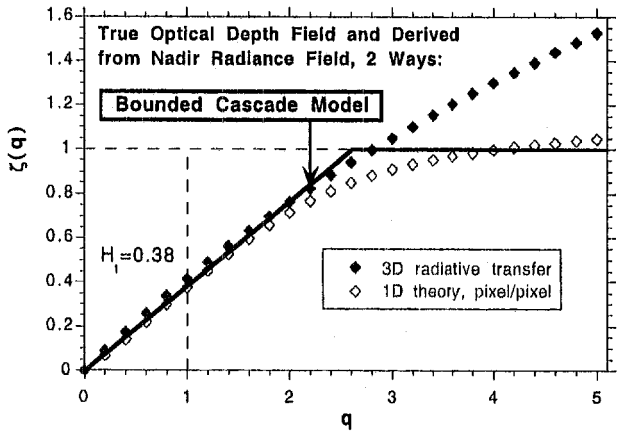

Figure 7: *Three exponent functions $\zeta(q)$ used in a study of cloud remote-sensing validation.* See text for details.

Figure 7 shows the function $\zeta(q)$, obtained by poor-man's wavelet analysis, for three different related fields. The solid curve is the theoretical $\zeta(q) = \min\{q/3,1\}$ for a random fractal cloud model using the bounded cascade described above and illustrated in Fig. 5. The empty symbols that hover close to this curve are what a remote-sensing analyst at (say) NASA would obtain using satellite reflectivities if only the radiative transfer was as simple in reality as he/she operationally assumes, namely, that each 0.3-0.5 km pixel is independent of the next. (This way, 1D vertical-only radiative transfer model can be used at each and every pixel.) The bold symbols that start close but end up far from the

theoretical curve that is targeted by the cloud remote sensing procedure are what is actually obtained in the presence of the complex 3D radiative transfer processes in clouds. This "apparent" scaling symmetry of the clouds is clearly wrong for high enough values of q and should be corrected in advanced applications.

3.2 Statistical Stationarity (in Time) or Homogeneity (in Space)

A lot of theory in the statistics of random processes is predicated on the assumption of stationarity (if the independent variable is time) or homogeneity (if it is space). The theoretical definition of a stationarity random process is that the values of all possible statistical quantities such as means, variances, wavelet coefficients, and so on, do not depend on when/where they are collected. In other words, they are invariant under translation or, equivalently, shift in origin (by operations in D_s and D_t). This definition is purely theoretical because, in practice, all the spatial information in the data is consumed in obtaining the statistical quantities in the first place, as explained above. So, in their wording, the theoreticians are clearly not referring to any particular finite dataset but to a vast functional probability space which contains all possible realizations of the random process, and that is where their operation of "ensemble-averaging" is conducted. For instance, the two sequences of 16 random digits used in Figs. 2 and 3 are just two realizations of that random process; a priori, there are 10^{16}-2 more realizations in that particular probability space.

Stationarity and homogeneity are still important notions in practical field work, so there has been a lot of work to help the data analysts decide whether their data is stationary or not. Recently, scale-invariance has been offered as a entry-point to this decision process by *Davis et al.* using wavelets *[1994a]* or more traditional techniques *[1994b]*. Moreover, these authors propose to use exponents, the main product os scale-invariance, as a means of measuring how stationary/homogeneous data is, or how far or close it is from being stationary/homogeneous (anticipating a subject of the next Section). In the remainder we will often mention stationarity and omit the homogeneity, and this is only for brevity; statements about the former concept carry over to the later unmodified. The distinction is theoretically important but can become moot in practice because often a spatial field is sampled by measurements in time anyway; for instance, a cloud probe on an aircraft (cf. Fig. 6a), or a fixed turbulence probe in a wind tunnel collect data in time.

Consider the data used in Figs. 3-4: sequences of 16 random digits between 0 and 9, most importantly here, they are mutually uncorrelated (drawn independently of their neighbors at any distance). This is a discrete "white-noise" process and it is patently stationary (in its probability space with a countable 10^{16} elements). The mean of this process is clearly 4.5 and it is not surprising that many of the Haar scaling function φ-coefficients cluster around this value, especially for the realization based on e in Fig. 3. This is true at all scales but with a spread that decreases as the scale increases; the realization based on π in Fig. 4 is more typical in this respect. Since the Haar wavelet ψ-coefficients at the next largest scale (down the binary tree in the figures) are simply the differences between neighboring φ-coefficients, they will and do decrease in magnitude as the scale increases. This can be generalized to other wavelets as they correspond to weighted rather than straightforward local averages of the data. What is the feature of the data that leads to the decrease of ψ-coefficients with scale? Clearly it is the rapid decorrelation between samples at different distances (in the white-noise case, the very next sample is already decorrelated). In turn, this decorrelation comes about from the excess of variability in the smallest scales.

So it is proposed that a decrease in the variance of ψ-coefficients with scale is the hallmark of stationarity. This operational definition of stationarity is useful to field workers with only a finite amount of data. In the framework of processes with the symmetry of scale-invariance, the additional symmetry of stationarity follows as soon as $\zeta_\psi(2) < 0$ in Eq. (4). (Technically speaking, this is "broad-sense" stationarity since it is based on a 2nd-order statistic but the argument can be generalized.) We can even propose that the more negative $\zeta_\psi(2)$ is, the more stationary are the data. The theoretical value of $\zeta_\psi(2)$ for uncorrelated noise is –1, so there are less and more stationary random processes. It is not just a true-false proposition as in the original definition.

This stationary situation with short-range decorrelation is also an example of exponent sensitivity to wavelet choice. While genuine wavelets yield $\zeta_\psi(2) = -1$ for white noise, the poor-man's wavelet that samples only two points at a given distance does no local averaging, so the theoretical exponent for any stationary process is $\zeta_\psi(2) = 0$. We have therefore lost the ability to distinguish more and less stationary data.

3.3 Statistical Isotropy (Invariance Under Rotation)

Our examples so far have used 1D data, functions of a single variable. This is by no means a limitation of the wavelet techniques or of the statistical concepts we have introduced. In fact, the contrary is true. In higher dimensions, we can define new symmetries to search for. This simplest is isotropy or statistical invariance under all possible rotations. Figure 8a shows a simple example in 2D: a reasonably symmetric cloud scene captured by LandSat, a NASA satellite carrying an imaging radiometer that looks straight down from space. The satellite is in a relatively low orbit from which it makes observations with considerable spatial detail (30-m pixels) by meteorological satellite standards (between 1/4- and 4-km pixels or larger). This 1980's technology has now been surpassed in the sense of spatial resolution with 5- and even 1-m pixels, at the cost of less spectral information however.

The key step is to generalize the wavelet shape from 1D to 2D and the simplest way to do this is to invoke symmetry by revolution. Figure 8b shows the so-called "Mexican Hat" wavelet. Mathematically inclined readers will recognize the 2nd radial derivative of a Gaussian surface. From there, the numerical recipes summarized in Eqs. (1-4) can be applied without any modification. The only problem occurs when trying to visualize the 3D data contained in a CWT of 2D input, but creative graphics can be used to see many scales at once *[e.g., Arrault et al., 1997]*.

The above procedure however assumes statistical isotropy rather than establishes it. To show that a field is statistically invariant under all 2D rotations in R_2, one needs (1) a wavelet that is not itself R_2-invariant and (2) to look at the angular decomposition of the results, say, for $q = 2$. Technical details are out of the scope of this survey and still a topic of ongoing research. Here again, the idea of looking first for scale-invariance and then for isotropy —or more subtle forms of rotational symmetry, as described by *Lovejoy and Schertzer [1986]*— is a promising avenue.

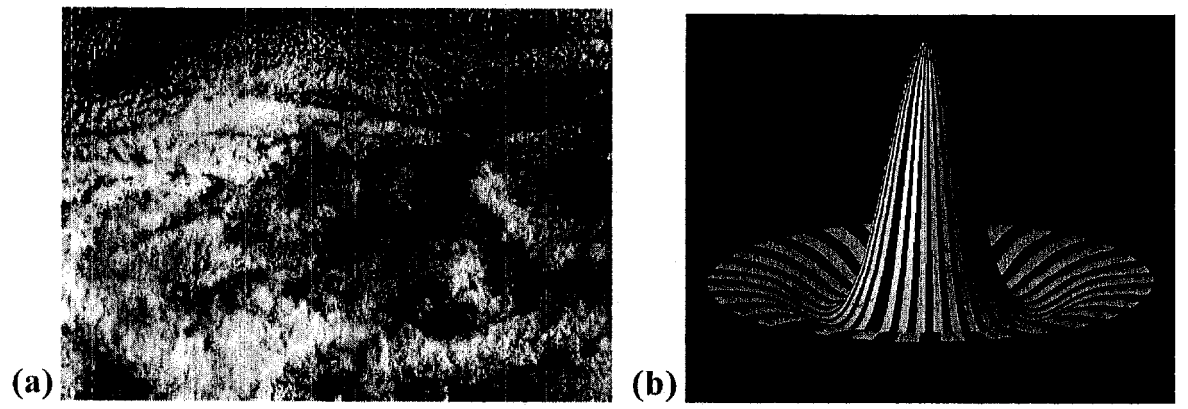

Figure 8: *Isotropic cloud field and a wavelet to analyze it.* **(a)** Portion of a LandSat cloud scene that is roughly isotropic with respect to rotations in 2D space. **(b)** The 2D "Mexican Hat" wavelet that goes as $(1-\rho^2)\exp(-\rho^2)$ where $\rho = (x^2+y^2)^{1/2}$ is the distance to the origin of the x- and y-axes.

4. STATISTICAL ASYMMETRIES, ILLUSTRATED WITH CLOUDS

4.1 Non-Stationarity (Inhomogeneity), with Stationary (Homogeneous) Increments

There is strong belief —largely based on symmetry principles— that Nature's variability patterns should be stationary in time (over time-scales that are short with respect to a global warming) and homogeneous in space (at least over climatically uniform areas). However, stationarity may be difficult, even impossible, to establish with data using the operational criterion presented in §3.2 because of Nature's propensity for very-long range correlations. In the case of clouds, the aircraft used to collect the in situ data used in section §3.1 may need to return to refuel before it has covered a complete decorrelation scale. Satellite coverage and continuous ground-based monitoring are better means to uncover homogeneity and stationarity respectively in atmospheric processes.

Consequently, it is paramount to consider statistical nonstationity and/or inhomogeneity. In the frame of processes with scale-invariant symmetry that obey Eq. (4), nonstationary/inhomogeneous behavior is present as soon as $\zeta(2) > 0$. This is the case for the bounded cascade model in Fig. 5. This is also the case for the internal cloud structure data in Fig. 6, a very typical situation in geophysics. Another way of qualifying this type of behavior found in the literature is "long-memory processes." At any rate, there is a sense of far more variability in the large scales than in the small ones which is in sharp contrast with stationary/homogeneous variability.

Following the same arguments in reverse as for the discrete white-noise model in §3.2, increasing wavelet coefficients with scale means that the scaling function coefficients, which are simply local averages, will fluctuate wildly from point to point in nonstationary data. This is somewhat unnerving for the field scientist that is out to determine the mean value of a quantity, so it is critically important in such work to characterize the correlations (that is "2-point" statistics or higher) in the data along with the mean (and all other "1-point" statistics such as variance or simply the histogram).

It is fair to say that only averages of stationary quantities can be certified as meaningful. If the data are stationary, then direct averaging is fine. Otherwise, it is important to find the stationary aspect of the data. In the above examples (bounded cascade and cloud structure), this is in the stationary "increments" that the wavelets are based on because they are required to oscillate at least once. So the symmetry properties of stationarity/homogeneity are in fact central to all statistical operations on data.

4.2 Statistical Anisotropy, or When One or More Directions are Special

In atmospheric dynamics, the NS and EW directions are not equivalent because of the Earth's rotation and also because of the solar illumination of one hemisphere at any given time. However, at small enough (much less than "synoptic") scales, a local form of isotropy can prevail at least some of the time, e.g., the cloud field in Fig. 8a. In contrast, the vertical direction is always radically different from horizontal ones in atmospheric structure. This is of course due to the Earth's strong gravitation that flattens the atmosphere into a very thin layer, only 10-12 km thick (using the highest clouds as a relevant marker) compared to its 6366 km radius (using 40000 km as a nominal circumference for the planet).

In a strongly anisotropic situation, such as the analysis of time-height fields of cloud radar reflectivity now obtained routinely by upward-looking ground-based instruments, anisotropic wavelets are in order. Figure 9a shows 3 steps of the geometrical cascade process used in a 2D anisotropic MRA based on the two wavelet bases illustrated in Fig. 1: the dyadic (Haar) basis in the vertical, and the triadic basis in the horizontal. We start with square pixels (presumably) at a scale much smaller than 10-12 km where the motions of air parcels have at least a chance to become isotropic. From there, we proceed to ever more flattened areas in the coarser representations, thus capturing to some extent the trend in atmospheric dynamics to stretch horizontally at scales comparable to 10-12 km. Figure 9b shows two cloud models obtained with the inverse anisotropic DWT in Fig. 9a, but for 3 more cascade steps, and some informed rules employing pseudo-random numbers *[Davis et al., 1999]*. In both realizations of the stochastic model, its parameters were tuned to give well-separated clouds in the vertical and long-range correlations in the horizontal direction, as observed in reality under quiescent atmospheric conditions. Convective storms are another matter altogether.

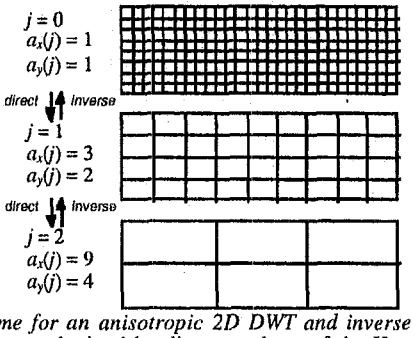

Figure 9a: *Multi-resolution analysis scheme for an anisotropic 2D DWT and inverse DWT.* The 6 piece-wise constant values for the 5 wavelets and one scaling-function are obtained by direct products of the Haar functions vertically and the triadic basis horizontally taken from Fig. 1, respectively l.- and r.-hand sides.

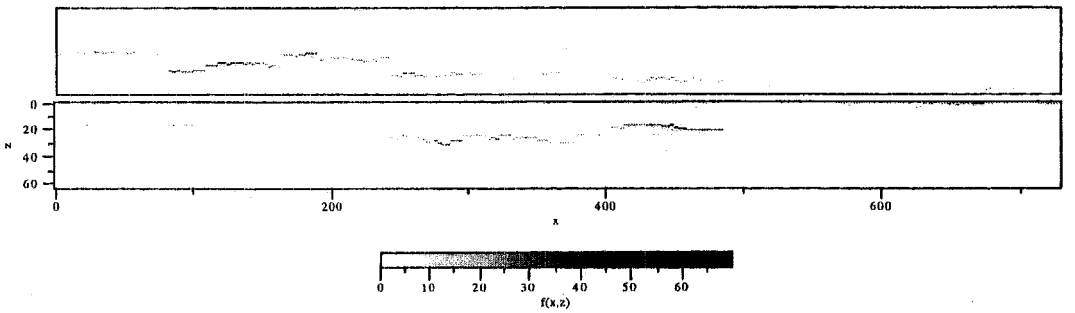

Figure 9b: *Two realizations of highly variable and strongly anisotropic cascades generated by inverse DWT, with unit mean.*

5. BROKEN SCALING SYMMETRY, ILLUSTRATED WITH CLOUDS

The most interesting data analysis exercises uncover a break in the dominant scaling symmetry. In the author's experience, this happens quite frequently, and sometimes two or three breaks occur. A break in scaling manifests itself as a distinct change in the slope of the log(*statistic*) vs. log (*scale*) plot exemplified in Fig. 6b. Figure 6b contains no such break because the deviations from a straight line there are erratic, due to limited sampling (only two realizations). A real break in scaling calls for a physical explanation. There are two different physics unfolding at the scales on either side of the break, and its position corresponds to a scale where different physics are in competition: it is a transition scale. Scale breaks are rarely sharp and sometimes are quite hard to see with limited and/or noisy data. However, when a break is clearly established, there is always something interesting to learn about the system or how it is being observed. Sometimes, the learning is about instrument performance, generally, it is about the natural process under observation. Whether the causality is artificial or natural, the break is often anticipated, but sometimes it is a surprise.

Figure 10 is a schematic that illustrates the different scale breaks anticipated in a typical experiment on turbulence using a statistical wavelet analysis of velocity, pressure, or temperature data that produces, say, $S_\psi(2;a)$ in Eq. (3). From classical turbulence phenomenology *[Frisch, 1995]*, one can anticipate three physically distinct regimes. At the largest scales, the data are decorrelated (so $S_\psi(2;a)$ decreases with scale) and it is stationary. At intermediate scales, the inertial physics of turbulence dominate and nonstationary behavior with $\zeta_\psi(2) = 2/3$ is observed. At a smaller but well-defined scale (that experts know as the "Kolmogorov scale"), the physics change from inertial to dissipative (these are literally the names of different terms in the evolution equations for fluid dynamics) and the flow becomes smooth and laminar. So, $\zeta_\psi(2)$ becomes 2 which is the maximum for this measure of nonstationarity, when positive. At the smallest scales, instrumental noise dominates over the now weak variability of the physical quantity; this noise is low-amplitude and decorrelated (if the instrument is well-built) so again we are in a stationary regime and $S_\psi(2;a)$ decreases with scale (the exponent $\zeta_\psi(2)$ is likely to be –1, the white-noise value). We have thus visited three physically interesting regimes and one instrument-dominated regime, hence three scale-breaks (including two where the exponent changes sign altogether).

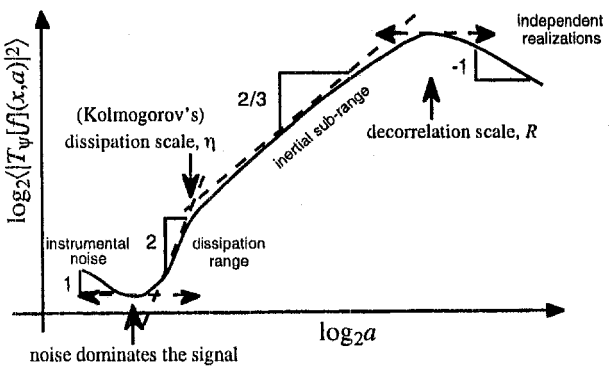

Figure 10: *Expected scale-breaks in a typical turbulence experiment using the wavelet energy spectrum.* See text for details.

Figure 11 shows the results of an extensive 3D radiative transfer simulation were cloud opacity (technically called "optical depth") varies horizontally as prescribed by a bounded cascade model tuned to reproduce observed cloud variability over three decades in scale, equivalently, 10 powers of 2 or "octaves." Figure 12 uses structure functions —the "poor-man's" wavelet analysis— to characterize the behavior scale-by-scale of simulated cloud radiance fields like those in Fig. 11, but as they would be observed from a satellite like LandSat (used for Fig. 8a). There is a clear scale-break between the 5th and 6th octaves. It goes from larger slopes $\zeta_\psi(q)$ at small scales associated with a smoother radiance field dominated by inter-pixel scattering to smaller slopes associated with a rougher radiance field that reflects —literally as well as figuratively— the turbulent structure of the cloud density field used in the simulation. For reference (dashed lines), Fig. 12 also shows the (unbroken) scaling obtained using a simpler pixel-by-pixel radiative calculation in Fig. 11. When this phenomenon was first uncovered empirically in LandSat cloud scenes such as Fig. 8a, there were equally compelling physical *[Cahalan and Snider, 1989]* and instrumental *[Lovejoy et al., 1993]* theories to explain the scale-break in the observations. However, this was all speculation. Once the break was obtained in simulations *[Davis et al., 1997]*, the physics were easy to figure out, with scattering between pixels playing a central role. So the two instrumental explanations were ruled out along with one of the physical theories, the final optical theory prevailed but not without a deep modification. The process is known in cloud optics as "radiative smoothing" *[Marshak et al., 1995]*.

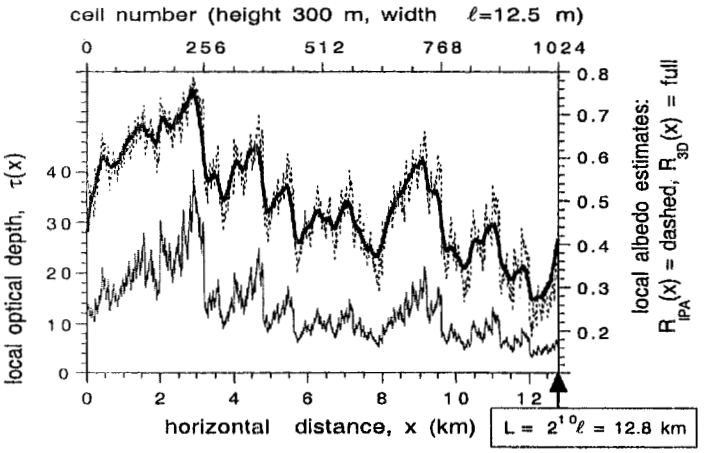

Figure 11: *Numerical simulation of the LandSat scale-break at 0.4 km due to multiple scattering between pixels.* Simulated radiance fields for a cloud model based on a bounded cascade also represented here; the (rough) dashed curve is for pixel-by-pixel computations (independent pixel approximation, or IPA) while the solid curve is for more realistic 3D radiative transfer.

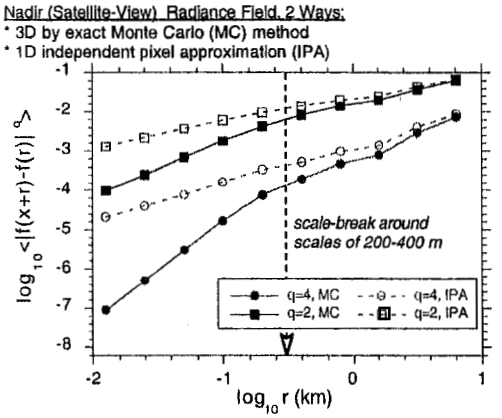

Figure 12: *Structure-function analysis of radiative smoothing.* Dashed curves are for the radiance field seen by a satellite computed pixel-by-pixel with a simple 1D vertical radiative transfer model. The bold lines are for a realistic computation using 3D radiative transfer. So the scale-break at around 300 m is direct evidence of 3D radiation transport effect mediated by the transport (via scattering) of sunlight between dense and adjacent tenuous pixels, a.k.a. radaitive smoothing, as seen in Fig. 11. The slopes for the large scales are used to obtain a few of the data points on Fig. 7.

6. SUMMARY AND OUTLOOK

I have showcased scaling concepts and demonstrated the power of wavelet implementations in our perennial quest to uncover regularity in Nature's behavior, even when it is apparently so erratic. Clouds were used to illustrate each step in the process of data collection and analysis that is followed, at least in some cases, by a net gain of physical insight into their complex dynamics and optics.

Symmetry is shown to be a guiding principle in this search, and statistics are the modality. Even so, we have used so far an essentially deterministic view of symmetry to find our way in the world of randomness, thus we defined statistical versions of translation-invariance, rotation-invariance, and zoom- or scale-invariance. We found these symmetries in Nature and we also found significant violations of each of these symmetries. So, although the term "symmetry" is rarely used in geophysical circles, it is deeply embedded in the culture of many geophysicists.

There are many extensions of the wavelet/fractal formalism presented here that incorporate more abstract statistical symmetries and asymmetries that have no obvious deterministic counterparts yet are related to important questions:

- multifractality (Are higher-order statistics related to their lower-order counterparts?);
- ergodicity (Is our operational space-time procedure for obtaining averages equivalent to ensemble-averaging?);
- log-periodicity (Is there a special dividing ratio in the cascade processes found in Nature?);

and so on.

A vigorous research program is in place to address these and other intellectually interesting questions and to bring them to bear on the most challenging issues in geophysical science. For instance, a problem of critical importance is that of extremes events in geophysics as well as in engineering. The highly nonlinear dynamics of geophysical processes is nowhere more threatening to human populations and natural ecosystems worldwide. Daily reports of floods, wildfires, landslides, hurricanes, tornadoes, earthquakes, volcanic eruptions, and so on, make extreme geophysics hard to ignore. Among all possible events, can one define a distinct component of extremes? Or are they just on a continuum with benign events? Can one characterize recognizable precursors to catastrophic extremes such as major earthquakes? What does "extreme" mean in a slowly changing climate? Are atmospheric extremes becoming more frequent and/or more intense in response to the trend global warming?

Acknowledgments

This work was funded in part by the Environmental Sciences Division of U.S. Department of Energy as part of the Atmospheric Radiation Measurement (ARM) program which also maintains the instrument-site from which the LWP data in Fig. 2. The FIRE data for airborne LWC used in Fig. 6, the LandSat data used in Fig. 8, as well as several model outputs, was obtained from Dr. Alexander Marshak at NASA's Goddard Space Flight Center and University of Maryland's Joint Center for Earth-science Technology (JCET). The author extends his appreciation to Drs. A. Arnéodo, R. Cahalan, E. Clothiaux, M. Farge, P. Flandrin, A. Fournier, K. Ivanova, S. Lovejoy, A. Marshak, M. Pal, N. Petrov, S. Roux, D. Schertzer, D. Sornette, and W. Wiscombe for many fruitful discussions about clouds, radiative transfer, fractals, wavelets and/or scale-invariance.

References

Albrecht, B. A., Randall, D. A., and Nicholls, S. (1988) Observations of marine stratocumulus clouds during FIRE, Bulletin of the American Meteorological Society, *69, 618-626.*

Arrault, J., Arnéodo, A., Davis, A. B., and Marshak, A. (1997) Wavelet-based multifractal analysis of rough surfaces: Application to cloud models and satellite data, Physical Review Letters, *79, 75-78.*

Barnsley, M. F. (1988) Fractals Everywhere. *San Diego (Ca): Academic Press, xii+394 pp.*

Cahalan, R. F., and Snider, J. B. 1989: Marine stratocumulus structure during FIRE, Remote Sensing of the Environment, *28, 95-107.*

Capra, F. (1991) The Tao of Physics. *3rd ed., updated, Boston (Ma): Shambhala Publ., 366 pp.*

Christakos, G. (1992) Random Fields in Earth Sciences. *San Diego (Ca): Academic Press, 474 pp.*

Daubechies, I. (1992) Ten Lectures on Wavelets. *Philadelphia (Pa): Society of Industrial and Applied Mathematics (SIAM), x+357 pp.*

Davis, A. B., Marshak, A., and Wiscombe, W. J. (1994a) Wavelet-based multifractal analysis of nonstationary and/or intermittent geophysical signals, In: Foufoula-Georgiou, E., and Kumar, P., eds. Wavelets in Geophysics, *San Diego (Ca): Academic Press, 249-298.*

Davis, A. B., Marshak, A., Wiscombe, W. J., and Cahalan, R. F. (1994b) Multifractal characterizations of nonstationarity and intermittency in geophysical fields: Observed, retrieved, or simulated, Journal of Geophysical Research, *99, 8055-8072.*

Davis, A. B., Marshak, A., Cahalan, R. F., and Wiscombe, W. J. (1997) The LANDSAT scale-break in stratocumulus as a three-dimensional radiative transfer effect, Implications for cloud remote sensing, Journal of the Atmospheric Sciences, *54, 241–260.*

Davis, A. B., Marshak, A., and Clothiaux, E. (1999) Anisotropic multi-resolution analysis in 2D, Application to long-range correlations in cloud mm-radar fields, In: Szu, H. H., ed. Wavelet Applications VI, S.P.I.E. Proceedings, Vol. 3723, *Bellingham (Wa): Publications of The Society of Photo-optical Instrumentation Engineers , 194-207.*

Fournier, A. (2000) Introduction to orthonormal wavelet analysis with shift invariance: Application to observed atmospheric blocking spatial structure, Journal of the Atmospheric Sciences, *57, 3856-3880.*

Frisch, U. (1995) Turbulence – The Legacy of A. N. Kolmogorov. *Cambridge (UK): Cambridge University Press, xiii+296 pp.*

Haar, A., 1910: Zur theorie der orthogonalen funktionesysteme, Math. Annal., *69, 331-371.*

Intergovernmental Panel on Climate Change (IPCC) (1996) Climate Change 1995: The science of climate change. *Houghton, J. T., et al. (eds.), London (UK): Cambridge Univ. Press, xii+572 pp.*

Lovejoy, S., and Schertzer, D. (1986) Scale invariance, symmetries, fractals and stochastic simulation of atmospheric phenomena, Bulletin of the American Meteorological Society, *67, 21–32.*

Lovejoy S., Schertzer, D., Silas, P., Tessier, Y., and Lavallee, D. (1993) The unified scaling model of atmospheric dynamics and systematic analysis of scale invariance in cloud radiances, Annales Geophysicae, *11, 119–127.*

Mallat, S. (1989) A theory for multiresolution signal decomposition: The wavelet representation, IEEE Transactions in Pattern Analysis and Machine Intelligence, *11, 674–693.*

Mallat, S. (1999) A Wavelet Tour of Signal Processing. *San Diego (Ca): Academic Press, xxiv+637 pp.*

Mandelbrot, B. B. (1982) The Fractal Geometry of Nature. *San Fransisco (Ca): W. H. Freeman, 460 pp.*

Marshak, A., Davis, A. B., Cahalan, R. F., and Wiscombe, W. J. (1994) Bounded cascade models as nonstationary multifractals, Physical Review E, *49, 55–69.*

Marshak, A., Davis, A. B., Wiscombe, W. J., and Cahalan, R. F. (1995) Radiative smoothing in fractal clouds, Journal of Geophysical Research, *100, 26247-26261.*

Monin, A. S., and Yaglom, A. M. (1975) Statistical Fluid Mechanics, Vol. 2. *Cambridge (Ma): MIT Press, 683 pp.*

Muzy, J.–F., Bacry, E., and Arnéodo, A. (1993) Multifractal formalism for fractal signals: The structure-function approach versus the wavelet-transform modulus-maxima method, Physical Review E, *47, 875-884.*

Muzy, J.–F., Bacry, E., and Arnéodo, A. (1994) The multifractal formalism revisited with wavelets, International Journal of Bifurcation and Chaos, *4, 245-302.*

Noether, E. A. (1918) Invariante variationsprobleme, Nachr. v. d. Ges. d. Wiss. zu Göttingen, *235-257, Trans. from German by M. A. Tavel (1971) Invariant variational problems,* Transport Theory and Statistical Mechanics, *vol. 1(3), 183-207.*

Sornette, D. (2000) Critical Phenomena in Natural Sciences – Chaos, Fractals, Self-organization and Disorder: Concepts and Tools. New York (NY): Springer-Verlag, xvii+434 pp.